Composites: Part A 41 (2010) 982-990

Contents lista abailable at scienceDirect

Composites: Part A

journal homepage: www.elsevier.com/lacate/compositesa

Processing and characterization of solid and microcellular PHBV/PBAT blend and its RWF/nanoclay composites

Alireza Javadi[a], Yottha Srithep[c], Jungjoo Lee[c], Srikanth Pilla[b], Craig Clemons[e], Shaoqin Gong[a,b,d],* Lih-Sheng Turng[c,]**

[a] Department of Materials, University of Wisconsin-Milwaukee, USA
[b] Department of Mechanical Engineering, University of Wisconsin-Milwaukee, USA
[c] Department of Mechanical Engineering, University of Wisconsin-Madison, USA
[d] Department of Biomedical Engineering, University of Wisconsin-Madison, USA
[e] Forest Products Laboratory, United States Department of Agriculture, Madison, WI, USA

ARTICLE INFO

Article history:
Received 17 February 2010
Received in revised form 27 March 2010
Accepted 2 april 2010

Keywords:
A. Polymer-matrix composites (PMCs)
B. Mechanical properties
C. Injection molding

ABSTRACT

Solid and microcellular components made of poly (3-hydroxybutyrate-*co*-3-hydroxyvalerate) (PHBV)/poly (butylenes adipate-*co*-terephthalate) (PBAT) blend (weight ration of PHBV:PBAT = 30:70), recycled wood fiber (RWF), and nanoclay (NC) were prepared via a conventional and microcellular-injection Molding process, respectively. Morphology, thermal properties, and mechanical properties were investigated. The addition of 10% RWF (both untreated and silate-treated) reduced the cell size and increased the cell density of the microcellular components. Also, the addition of 10% RWF (both untreated and silane-treated) generally increased the specific Young's modulus and tensile strength, but decreased the specific toughness and strain-at-break in both solid and microcellular components. Moreover, unlike the near PHBV/PBAT blend, microcellular PHBV/PBAT/RWF (both untreated and silane-treated) composites showed higher specific toughness and strain-at-break compared to their solid counterparts. In addition, higher specific toughness and strain-at-break was observed in the PHBV/PBAT/untreated-RWF composite compared with the PHBV/PBAT/silane-treated RWF composite, particularly in the microcellu-Lar components. The degree of PHBV crystallinity increased significantly in both solid and microcellular PHBV/PBAT/RWF composites although the degree of PHBV crystallinity in the solid components was Slightly higher than that of their microcellular counterparts. The effects of adding 2% nanoclay on the properties of the PHBV/PBAT/silane-treated-RWF composite were also investigated. The nanoclays exhibited an intercalated structure in the composites based on XRD analysis and did not induce significant changes in cell morphology and mechanical properties of the PHBV/PBAT/silane-treated-RWF composite. However, it did improve its thermal stability.

© 2010 Elsevier Ltd. All rights reserved.

1. Introduction

Biobased and biodegradable polymers such as polyhydroxyalkanoates (PHAs) and polylactide (PLA) have attracted much attention over the last two decades mainly due to increasing environmental concerns and the realization that our petroleum resources are finite [1]. PHAs are a family of polyesters that are synthesized and intracellularly accumulated as a carbon and energy storage material in various microorganisms [2,3]. Poly(hydroxybutyrate-*co*-hydroxyvalerate)(PHBV), a member of the family of PHAs, has gained a lot of attention because of its biodegradability and biocompatibility and the similarities of its mechanical properties to those of polyolefins such as polypropylene [4]. These remarable features make PHBV a potential substitute for petroleum-based polyolefins in many areas such as the automotive industry and biomedical applications [5]. However, widespread application of PHBV is limited because of its high cost and certain inferior material properties such as brittleness and low impact resistance [6].

Blending PHBV with toughened polymers is a practical and economical way to improve its inferior mechanical properties. To this effect, PHBV was blended with polystyrene, poly(ethylene oxide), polycaprolactone, poly(propylene carbonate), starch, poly(styrene-*co*-acrylonitrile), starch-graph-poly(glycidyl methacrylate) and poly (butylenes adipate-*co*-terephthalate)(PBAT) [7-14]. In our previous study, blending PHBV with PBAT improved the specific toughness

*Corresponding author at: Department of Biomechanical Engineering, University of Wisconsin-Madison, USA.
**Corresponding author.
E-mail addresses: shaoquingong@wisc.edu (S. Gong), turng@engr.wisc.edu (L.-S. Turng).

1359-835X/$ - see front matter © 2010 Elsevier Ltd. All rights reserved
doi: 10.1016/j.compositesa.2010.04.002

up to two orders of magnitude for solid and microcellular specimens compared to neat PHBV [14]. Also, the PHBV/PBAT blend showed a more than 500% increment in strain-at-break for both solid and microcellular samples compared to neat PHBV [14]. However, the dramatic increase in toughness and strain-at-break observed in the PHBV/PBAT blends were accompanied by an apparent reduction in strength and modulus compared with pure PHBV [14]. Typically, thestrengthandstiffness of a polymer can be improved by adding certain types of fillers. Fillers can be classified as natural and synthetic. Natural fillers, including wood fibers, offer several advantages such as biodegradability, renewability, low cost, low density. high specific strengthand stiffness, andlesswear onmachinery [15–18]. However, they tend to exhibit low thermal stability [19]. To improve the thermal stability, inorganic nanofillers such as nanoclays were investigated by several groups [20,21]. It was found that the incorporation of nanoclay to wood/polymer composites systems resulted in a decrease in the thermalexpansioncoefficient andanincreaseinthe heat deflectiontemperature [20] and Young's modulus as well as increased thermal stability [21]. In the present study, both natural fillers (recycled wood fibers (RWF)) and synthetic fillers (nanoclays) were incorporated into the PHBV/PBAT blend to produce hybrid biocomposites with superior material properties. To provide good interfacial adhesion between hydrophilic wood fibers and hydrophobic PHBV, the RWF were pre-treated with silane.

Microcellular components made of four different formulations (Ref. Table 1) were produced via microcellular injection-molding using supercritical nitrogen fluid as the physical foaming agent. During the microcellular injection-molding process, the SCF is injected into the polymer melt inside the injection-molding barrel to form a single-phase polymer–gas solution. A sudden pressure drop occurring at the nozzle or near the gate induces a thermodynamic instability in the polymer–gas solution, triggering cell nucleation and growth. Components produced by microcellular injection molding possess excellent dimensional stability. lower total cost due to the use of less materials and shorter cycle time [22–26]. This is very desirable for biobased polymers especially PHBV because of their high cost compared to synthetic polymers. Additionally, microcellular components with a large number of small and uniform microcells may exhibit higher toughness as microcells can act as "crack arrestors" which is an attractive feature for brittle biobased materials such as PHBV [22–26]. For comparison, solid components were also produced via the conventional injection-molding process.

The objective of this study was to achieve an overall improvement of the mechanical and thermal properties of PHBV-based biocomposites using a unique microcellular injection-molding processing technology.

2. Experimental

2.1. Materials and processing conditions

The PHBV/PBAT blend was purchased, in pellet form, from Ningbo Tianan Biologic Material Co. Ltd., (Tinan-ENMAT) (China) under the trade name 6010P with a weight ratio between PHBV and PBAT of 30:70. GE Silicones Silquest A-174® silane (gamma-methacryloxypropyltrimethoxysilane). obtained from Witco Corp., was used as the coupling agent. The chemical formula for silane is given as $CH_2{=}C(CH_3)\ CO_2CH_2CH_2CH_2Si\ (OCH_3)_3$. Nanoclay under the trade name Cloisite® 30B was bought from Southern Clay products and RWF was bought from American Wood Fibers, WI, USA.

A kinetic mixer (K-mixer; Vanzetti Systems Series 3009) was used to blend the PHBV/PBAT, RWF, and/or nanoclay depending on the formulation. The K-mixer was turned on and once it reached around 150 °C. it was turned off. After discharging, the molten blend was hot-pressed into a flat sheet and subsequently granulated. The blends were then dried at 80°C for 24h. Solid and microcellular components were injection-molded using an Arberg All rounder 320S (Lossburg, Germany) with a 25 mm diameter screw and equipped with Mucell® technology (trexel, Inc., Woburn, MA). The processing conditions for conventional injection molding and microcellular injection molding are presented in Table 1.

2.2. Methods

Various techniques have been used to evaluate the mechanical, thermal, and morphological properties.

2.3. Tensile testing

The tensile properties (modulus, strength, toughness, and elongation at break) were measured at room conditions using a 5 kN load cell on an Instron Model 5566 tensile tester. The extension was set at 25.4 mm/min. All tests were carried out according to the ASTM standard (ASTM-D638). Five specimens of each sample were tested and the average results with standard deviation were reported.

2.4. Dynamic mechanical analysis (DMA)

The DMA experiments were carried out using a dynamic mechanical analyzer (DMA Q800, TA instruments). Rectangular specimens with a dimension of approximately 17.6 by 12.7 by 3.2 mm^3 were cut from injection molded parts and were tested in a single-cantilever mode. The heating rate was 3 °C/min from −50°C to 80 °C with 1 Hz frequency and 0.02% pre-strain, which was in the linear viscoelastic region as determined by a strain sweep.

2.5. Differential scanning calorimetry (DSC)

Thermal properties were determined using a DSC (TA instruments, Auto DSC Q20). The weight of the DSC samples was around 7–9 mg. Samples were first heated from 40 °C to 200 °C. kept isothermal for 3 min at 200 °C. cooled down to −50°C. and then reheated to 200 °C. The ramp rate for all the heating and cooling cycles was 10 °C/min. The crystallization temperature (T_c), melt

Table 1
Injection molding parameters for the four formulations listed in this table.

Sampler		Mold temperature (°C)	Nozzle temperature (°C)	Pack pressure (MPa)	Pack time (s)	Shot volume (cm^3)
PHBV/PBAT	Solid	20	180	80	4	20.5
	Microcellular	20	190	0	0	20
PHBV/PBAT + 10% untreated-RWF	Solid	20	170	80	4	19.8
	Microcellular	20	190	0	0	20
PHBV/PBAT + 10% silane-treated-RWF	Solid	20	170	80	8	19.8
	Microcellular	20	190	0	0	20
PHBV/PBAT + 10% silane-treated-RWF + 2% nanoclay	Solid	20	170	100	8	20.6
	Microcellular	20	190	0	0	20.4

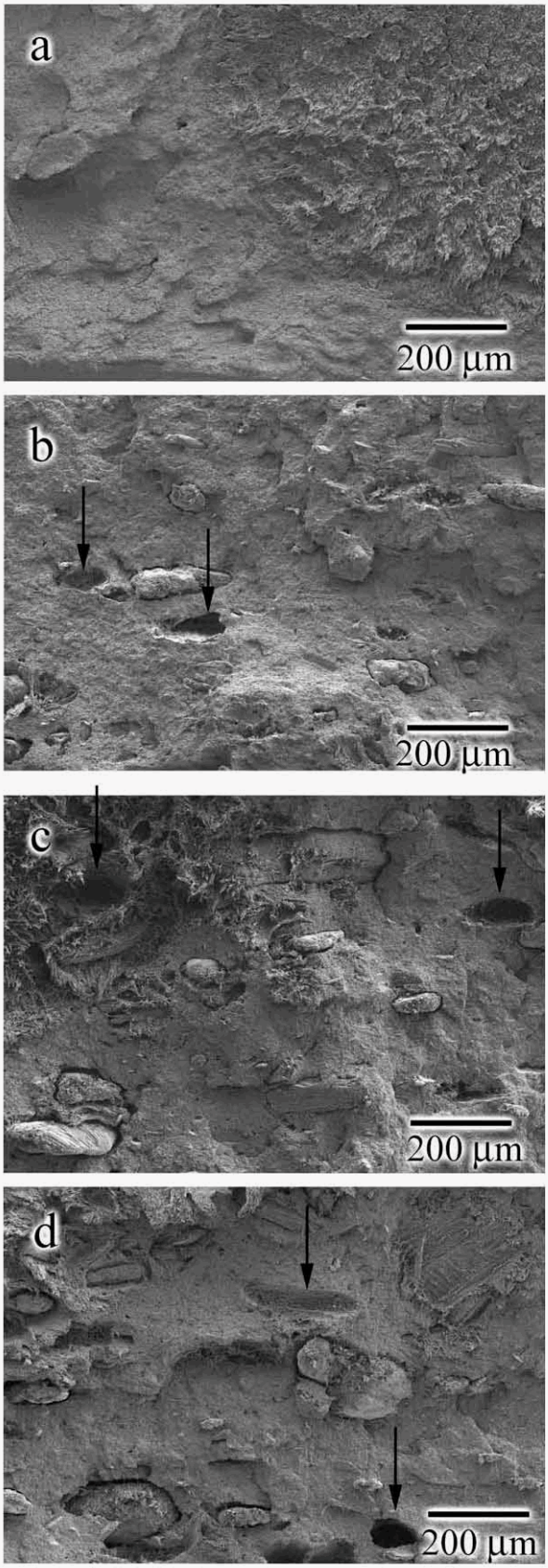

Fig. 1. Tensile fractured surfaces of the solid components made of (a) PHBV/PBAT blend; (b) PHBV/PBAT/untreated-RWF composite; (c) PHBV/PBAT/silane-treated-RWF composite; (d) PHBV/PBAT/silane–treated-RWF/nanoclay composite.

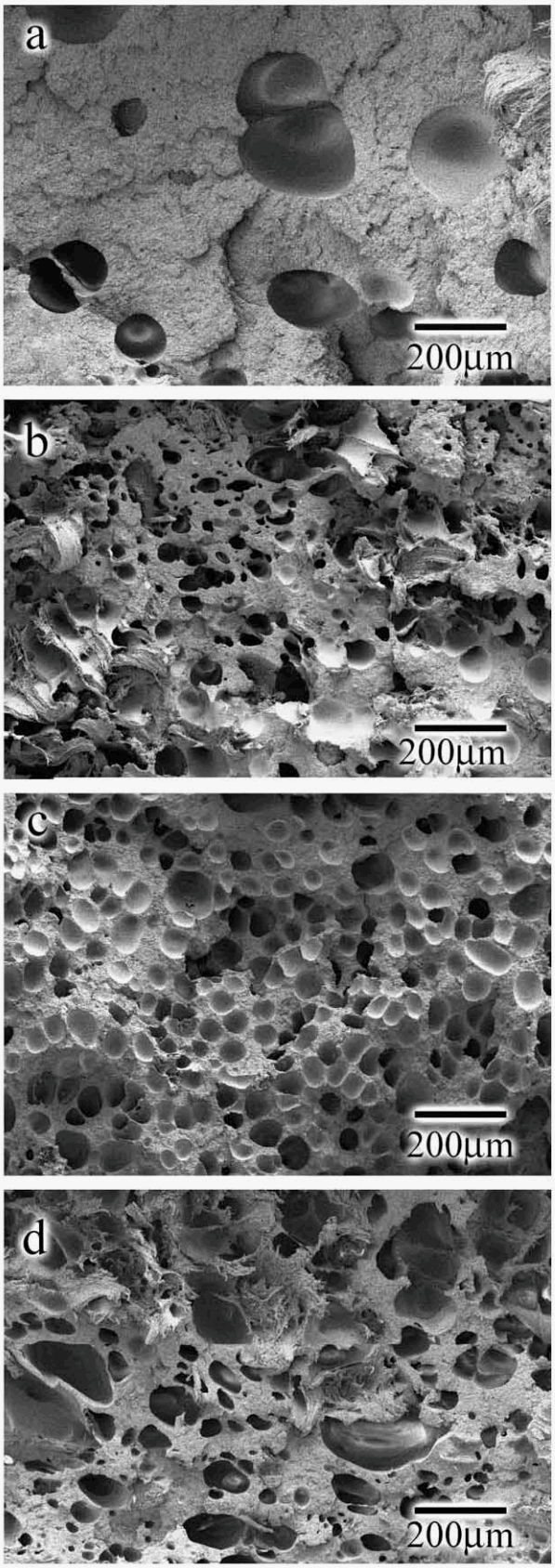

Fig 2 Tensile fractured surfaces of microcellular components made of (a) PHBV/PBAT blend, (b) PHBV/PBAT/untreated-RWF composite, (c) PHBV/PBAT/silane-treated-RWF composite and (d) PHBV/PBAT/silane-treated- RWF/nanoclay composite.

temperature (T_m), apparent melting enthalpy (ΔH_f), and enthalpy of crystallization (ΔH_{cc}) were determined from the DSC curves. T_m and ΔH_f were taken as the peak temperature and the area of the melting endotherm, respectively.

The crystallinity (χ_c) of the PHBV phase was calculated by

$$\chi_c(\%) = \frac{\Delta H_f(\mathrm{PHBV})}{\Delta H^0(\mathrm{PHBV})} \times \frac{100}{w} \quad (1)$$

where ΔH(PHBV) is the enthalpy of melting per gram of 100% crystalline (perfect cystal) (109 J/g) and w is the weight fraction of PHBV in the blend [27].

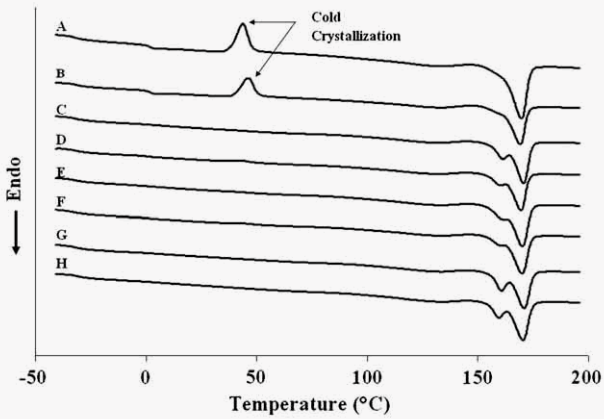

Fig. 3. Melting curves of solid and microcellular PHBV/PBAT blend and PHBV/PBAT/RWF/nanoclay composites obtained from the second heating run: (A) PHBV/PBAT blend (solid): (B) PHBV/PBAT blend (microcellular); (C) PHBV/PBAT/untreated-RWF composite (solid): (D) PHBV/PBAT/PHBV/PBAT/untreated-RWF composite (microcellular); (E) PHBV/PBAT/silane-treated-RWF composite (solid): (F) PHBV/PBAT/silane-treated-RWF composite (microcellular): (G) PHBV/PBAT/silane-treated-RWF/nanoclay composite (solid): and (H) PHBV/PBAT/silane-treated-RWF/nanoclay composite (microcellular).

Table 2
Representative values of the average cell size and cell density of the microcellular PHBV/PBAT blend and its RWF/nanoclay composites.

Samples	Avg. cell size	Cell density (number/cm³)
PHBV/PBAT	239 ± 310	2.56E + 04
PHBV/PBAT + 10% untreated-RWF	61 ± 32	2.50E + 06
PHBV/PBAT + 10% silane-treated-RWF	57 ± 16	2.87E + 06
PHBV/PBAT + 10% silane-treated-RWF + 2% nanoclay	73 ± 48	1.89E+06

To determine the crystallinity of the sample, the extra heat absorbed by the crystallites formed during heating (i.e., cold crystallization) had to be subtracted from the total endothermic heat flow due to the melting of the whole crystallites [28]. Thus, the modified equation can be written as follows:

$$\chi_c(\%\ \mathrm{Crystallinity}) = \frac{\Delta H_f(\mathrm{PHBV}) - \Delta H_{cc}(\mathrm{PHBV})}{\Delta H^0(\mathrm{PHBV})} \times \frac{100}{w} \quad (2)$$

2.6. Wide-angle X-ray diffraction (WAXRD)

A WAXRD analysis was performed using Scintag XDS 2000 with Ni-filtered Cu Kα radiation (1.5418 A°) at room temperature in the range of 2θ = 1.5–40° with a scanning rate of 2°/min.

2.7. Thermo gravimetric analysis (TGA)

Thermo gravimetric analysis (TGA) and derivative thermo gravimetric analysis (DTG) tests were performed using a SDT 2960 thermo gravimetric analyzer (TA Instruments) from 50 °C to 600°C with a heating ramp of 20°C/min under Argon flow (100 cm³/min).

2.8. Scanning electron microscopy (SEM)

SEM images of the tensile fractured surfaces of injection-molded specimens were obtained using an ultra high resolution FE-SEM (Hitachi S-4800) operated at 4 kV. All specimens were sputter-coated with a thin layer of gold–palladium (5 nm) prior to examination. The comparison between the SEM images of the different specimens was made at the same magnification.

Analysis of the average cell size and cell density was performed quantitatively using an image analysis tool (UTHSCSA image tool). The cell density was calculated using the following formula [29]:

$$\text{Cell density} = \left(\frac{N}{L^2}\right)^{1.5} \times \mathrm{M} \quad (3)$$

where N is the number of cells, L is the linear length of the area, and M is a unit conversion resulting in the number of cells per cm³.

3. Results and discussion

3.1. Morphology of the fractured surfaces of both solid and microcellular components

Figs. 1 and 2 show the SEM images of the PHBV/PBAT blend and its RWF/nanoclay composites. Both solid and microcellular samples were investigated. As can be seen from the images shown in Fig. 1, the tensile fractured surfaces of the solid PHBV/PBAT blend

Table 3
Thermal characteristics of the solid and microcellular PHBV/PBAT blend and its RWF/nanoclay composites obtained from the second heating run

Sample	1st cold crystallization (first heating)		Melting (first heating)			Crystallinity
	Temperature (°C)	Enthalpy (J/g)	Temperature (°C)		Enthalpy (J/g)	
Solid						
PHBV/PBAT	43.8	9.3	169.6		23.5	43
PHBV/PBAT + 10% untreated-RWF	N/A	N/A	161.4	170.6	18.7	63
PHBV/PBAT + 10% silane-treated-RWF	N/A	N/A	161.9	170.2	18.7	63
PHBV/PBAT + 10% silane-treated-RWF + 2% nanoclay	N/A	N/A	160.7	170.8	19.3	66
Microcellular						
PHBV/PBAT	46.2	5.9	169.2		16.5	32
PHBV/PBAT + 10% untreated-RWF	N/A	N/A	159.5	169.5	17.5	59
PHBV/PBAT + 10% silane-treated-RWF	N/A	N/A	1621	170	17.6	59
PHBV/PBAT + 10% silane-tretaed-RWF + 2% nanoclay	N/A	N/A	159.5	170.4	18.0	62

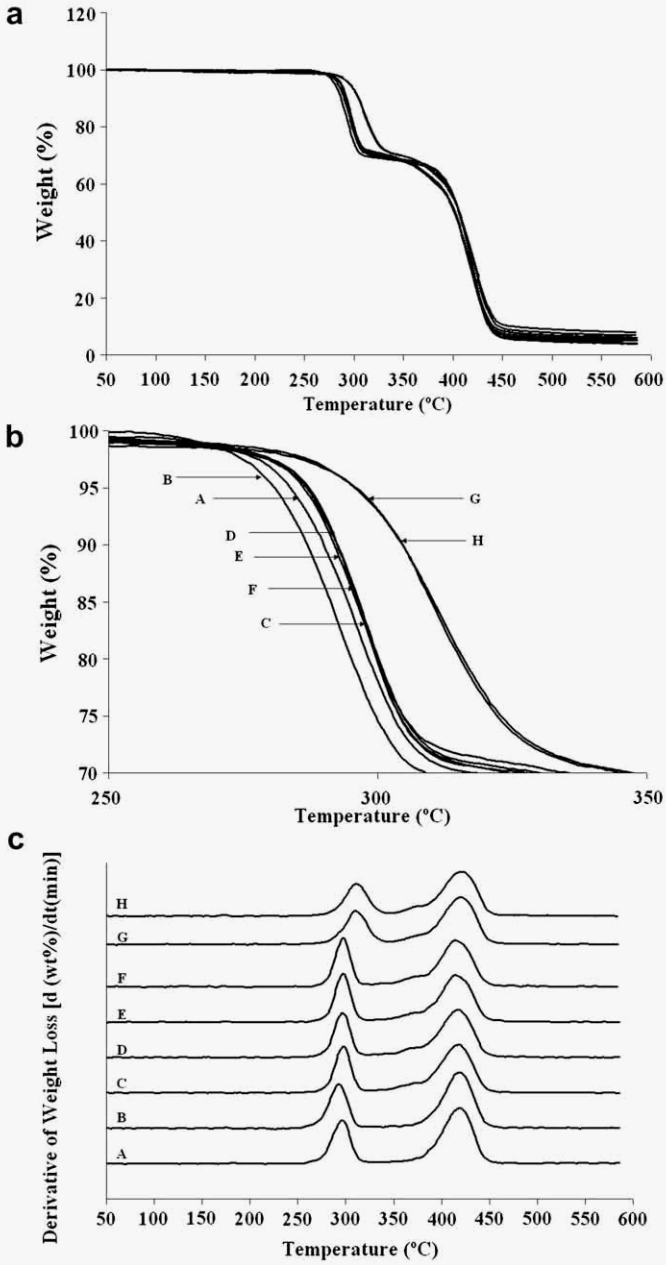

Fig. 4. (a) and (b) Weight loss of PHBV/PBAT blend and its RWF/nanoclay composites with temperature, (c) DTG curves with temperature: (A) PHBV/PBAT blend (solid): (B) PHBV/PBAT blend (microcellular); (C) PHBV/PBAT/untreated-RWF composite (solid): (D) PHBV/PBAT/PHBV/PBAT/untreated-RWF composite (microcellular): (E) PHBV/PBAT/silane-treated-RWF composite (solid); (F) PHBV/PBAT/silane-treated-RWF composite (microcellular); (G) PHBV/PBAT/silane-treated-RWF/nanoclay composite (solid): and (H) PHBV/PBAT/silane-treated-RWF/nanoclay composite (microcellular).

and its RWF/nanoclay composites components were relatively rough, indicating that all of the samples fractured under the ductile mode. This observation was supported by the values of specific toughness and strain-at-break obtained from the tensile tests. In Fig. lb, a few fiber pull-out spots (depicted by black arrows) were observed at the tensile fractured surface of untreated-RWF composite. The tensile fractured surfaces of silane-treated-RWF (Fig. 1c and d) did not show any significant change in the number of fiber pull-out spots (depicted by black arrows) which implies that the silane-treatment did not have any noteworthy effect in improvement of fiber–matrix adhesion [30].

Fig. 2a–d shows the representative images of the tensile fractured surface of the microcellular PHBV/PBAT blend, PHBV/PBAT/untreated-RWF composite, PHBV/PBAT/silane-treated-RWF composite, and PHBV/PBAT/silane-treated-RWF/nanoclay composite, respectively.

A quantitative analysis of the average cell size and cell density was performed using an image analysis tool (UTHSCSA Image Tool) and the results are summarized in Table 2. Quantification of the cellular structure was done from the center portion of the cross-section of the tensile bars. Variations in cell size and cell density occur throughout the thickness of the part due to shear and rapid cooling at the polymer–mold interface.

As shown in Table 2, the addition of both silane-treated and untreated-RWF decreased the cell size of the microcellular PHBV/PBAT by three times and increased the cell density by approximately two orders of magnitudes. This shows that the RWF can effectively serve as a nucleating agent for microcells, thereby promoting energy-favorable heterogeneous nucleation which can also lead to more uniform growth besides a higher cell density and low cell size [31,32]. Silane-treatment on the RWF did not induce a significant difference in the average cell size and cell density; however, it was noted that the cell size of the microcellular PHBV/PBAT/silane-treated-RWF composite appeared more uniform than that of the microcellular PHBV/PBAT/untreated-RWF composite. Finally, adding 2% nanoclay to the PHBV/PBAT/silane-treated-RWF composite led to a less uniform cell morphology

3.2. Thermal properties

3.2.1. Crystallinity

Crystallization behaviors were studied using DSC. Fig. 3 shows the thermograms obtained from the second heating cycle. Table 3 shows the numerical values of the temperature and enthalpy obtained from the second heating cycle and the degree of crystallinity for the PHBV/PBAT blend and its RWF/nanoclay composites.

As can be seen in Fig. 3, for both the solid and microcellular components, while the PHBV/PBAT blends showed a single melting peak, the PHBV/PBAT composites exhibited double melting peaks. This may be attributed to different types of crystalline structures or a variation in thickness of the lamellar structure and size of the spherulites obtained during the crystallization process of the

Table 4
The initial degradation temperatures, the DTG peak temperatures, and the ash contents of the PHBV/PBAT blend and its RWF/nanoclay composites.

Sampler		Initial degradation temperatures (°C)		DTG peak temperatures (°C)		Ash content (%)
		PHBV	PBAT	PHBV	PBAT	
PHBV/PBAT	Solid	270.6	392.5	296.4	419.7	4.0
	Microcellular	278.4	394.2	293.1	419.3	3.8
PHBV/PBAT + 10% untreated-RWF	Solid	284.4	392.9	297.6	418.6	5.0
	Microcellular	285.4	393.3	296.9	417.8	5.3
PHBV/PBAT + 10% silane-treated-RWF	Solid	286.9	395.3	297.4	414.5	6.1
	Microcellular	287.0	394.8	297.4	414.6	5.7
PHBV/PBAT + 10% silane-treated-RWF+ 2% nanoclay	Solid	297.0	397.1	310.1	419.9	7.0
	Microcellular	296.7	391.8	311.2	421.3	7.6

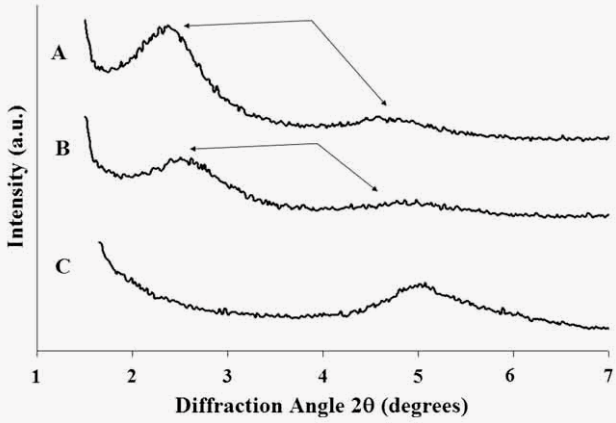

Fig. 5 Wide-angle XRD patterns of (A) PHBV/PBAT/silane-treated-RWF/nanoclay. composite (solid); (B) PHBV/PBAT/silane-treated-RWF/nanoclay composite (microcelular); (C) nanoclay (Cloisite® 30B).

composites [25,33]. Also. cold crystallization peaks were observed for neat PHBV/PBAT blends. However, the cold crystallization peaks vanished for composite specimens indicating that there were no more amorphous regions that had the ability to crystallize in those samples [24].

Table 3 shows the degree of crystallinity (χ) of PHBV in the filled composites for solid and microcellular components obtained from the second heating cycle. The addition of 10% untreated and silane-treated RWF increased the degree of the crystallinity by 20% and 27% for the solid and microcellular samples, respectively. This may be attributed to the fact that RWF acted as a crystallization nucleating agent [19]. The addition of 2% nanoclay further increased the degree of crystallinity of the PHBV/PBAT/silane-treated RWF composites by 3% for both solid and microcellular samples. Furthermore, at the same blend composition, microcellular components showed a lower degree of crystallinity compared to their solid counterpart.

3.2.2. Thermo gravimetric analysis

The thermal stability of the PHBV/PBAT blend and its RWF/nanoclay composites were studied using TGA. Fig. 4a and b depict the weight loss of the PHBV/PBAT blend and its RWF/nanoclay composites with temperature. Fig. 4b is a magnified version of Fig. 4a in the first major weight loss area. As can be seen from the TGA curves. two major weight loss steps were observed for all samples. According to the literature [34,35]. the first andsecond major weight losses are attributed to PHBV and PBAT, respectively. The difference in thermal decomposition behavior of the samples can be seen more clearly from the derivative TG (DTG) curves (Fig. 4c) which show the derivatives of weight loss with respect to time [*dw/dt* (min)]. As can be seen, the DTG curves show double peaks for all samples – which indicate thermal degradation - consisted of two major weight loss steps. The peak temperatures i.e., the mid-points of the degradation at each major step, are a measure of thermal stability [34,36,37]. The initial degradation temperatures, the peak temperatures obtained by DTG, and the ash content are reported in Table 4. As can be observed, the addition of 10% untreated and silane-treated RWF did not shift the DTG peak to a higher temperature compared to the neat PHBV/PBAT blend for both solid and microcellular components. However, the PHBV/PBAT/silane-treated RWF/nanoclay composites exhibited a higher DTG peak temperature and initial degradation temperature than the PHBV/PBAT/silane-treated RWF composites in both solid and microcellular components. The increase in thermal stability

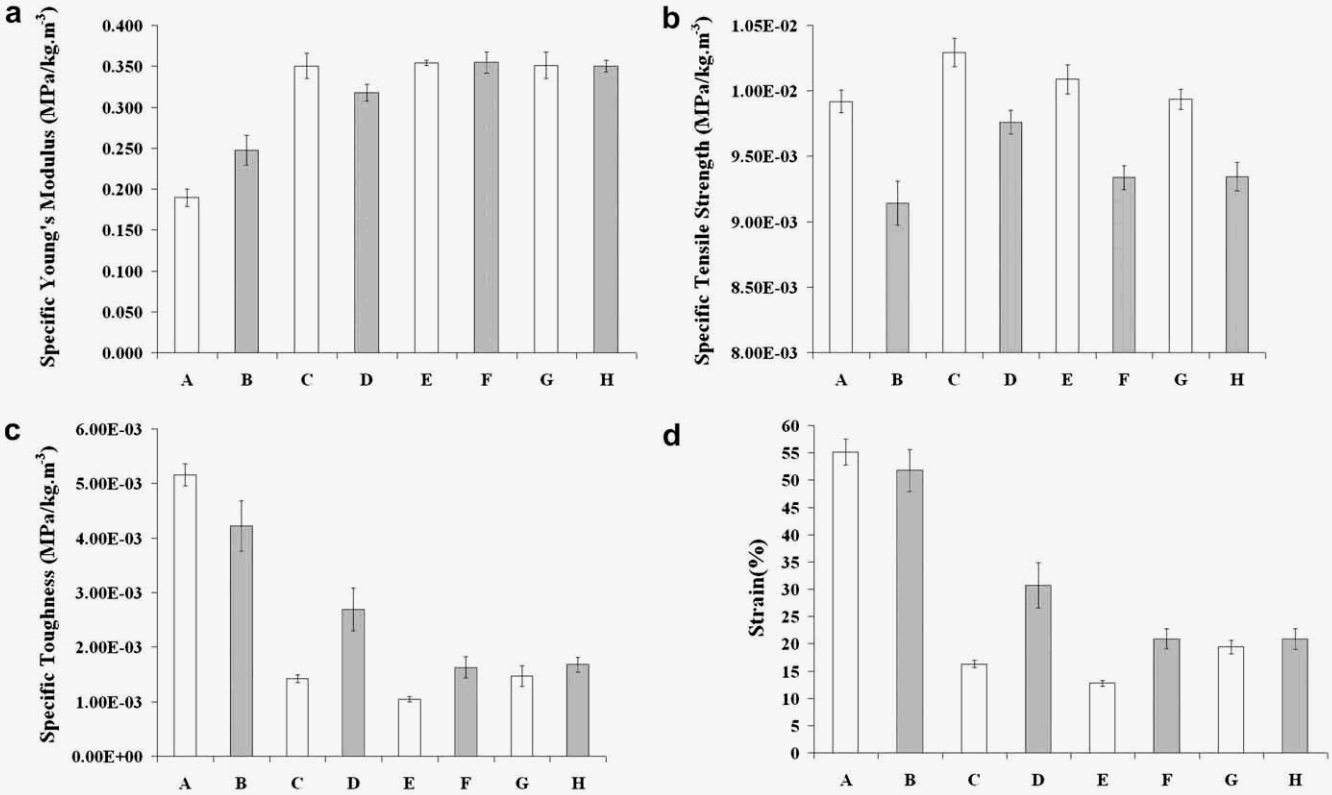

Fig. 6. Specific mechanical properties of solid and microcellular PHBV/PBAT and its RWF/nanoclay composites; (a) specific Young's modulus (MPa/kg m³): (b) specific tensile strength (MPa/kg m³): (c) specific toughness (MPa/kg m³): (d) strain-at-break(%). (A) PHBV/PBAT blend (solid): (B) PHBV/PBAT blend (microcellular): (C) PHBV/PBAT/untreated-RWF composite (solid): (D) PHBV/PBAT/PHBV/PBAT/untreated-RWF composite (microcellular): (E) PHBV/PBAT/silane-treated-RWF composite (solid): (F) PHBV/PBAT/silane-treated-RWF composite (microcellular): (G) PHBV/PBAT/silane-treated-RWF/nanoclay composite (solid): and (H) PHBV/PBAT/silane-treated-RWF/nanoclay composite (microcellular).

Table 5
Specific mechanical properties of solid and microcellular PHBV/PBAT blend and its RWF/nanoclay Composites.

Sample		Specific toughness (MPa/kg m³)	Strain-at -break(%)	Specific Young's modulus (MPa/kg m³)	Specific tensile strength (MPa/kg m³)
PHBV/PBAT	Solid	5.2E−3 ± 2.1E−4	55.1 ± 2.4	1.9E−1 ± 1.1E−2	9.9E−3 ± 8.6E−5
	Microcellular	4.2E−3 ± 6.4E−4	51.8 ± 3.8	2.5E−1 ± 1.8E−2	9.1E−3 ± 1.7E−4
PHBV/PBAT+10% untreated-RWF	Solid	1.4E−3 ± 7.0E−5	16.3 ± 0.6	3.5E−1 ± 1.5E−2	1.0E−2 ± 1.1E−4
	Microcellular	2.7E−3 ± 3.9E−4	30.7 ± 4.2	3.2E−1 ± 1.0E−2	9.8E−3 ± 9.2E−5
PHBV/PBAT+10% silane-treated-RWF	Solid	1.0E−3 ± 5.1E−5	12.8 ± 0.5	3.5E−1 ± 2.9E−3	1.0E−2 ± 1.1E−4
	Microcellular	1.6E−3 ± 2.0E−4	20.9 ± 1.9	3.5E−1 ± 1.3E−2	9.3E−3 ± 9.1E−5
PHBV/PBAT+10% silane-treated -RWF+2% nanoclay	Solid	1.5E−3 ± 1.9E−4	19.4 ± 1.3	3.5E−1 ± 1.6E−2	9.9E−3 ± 7.7E−5
	Microcellular	1.7E−3 ± 1.4E−4	20.8 ± 1.9	3.5E−1 ± 7.3E−3	9.3E−3 ± 1.1E−4

observed with the addition of layered silicates in biopolymers arises from fact that nanoclays can act as a heat barrier, thereby increasing the thermal stability of the system [38]. Furthermore, with the addition of untreated and silane-treated RWF. the ash content increased for both solid and microcellular specimens. This might be attributable to the presence of certain minerals in RWF which do not decompose at higher temperatures. With the addition of nanoclay. the ash content increased further as a major portion of nanoclay consists of silicates [38,39].

3.3. Wide-angle X-ray diffraction analysis

The structure of polymer composites was studied using wide-angle XRD which provides a convenient way to determine the degree of clay intercalation by monitoring the position, shape, and intensity of the (0 0 1) diffraction peak from the dispersed nanoclays. The interlayer distance after intercalation was calculated from the angular position 28 using the Bragg formula, $\lambda = 2d \sin\theta$ (wavelength (A) of the X-ray was 0.154 nm) [40].

As can be seen in Fig. 5, the (0 0 1) peak for nanoclay (Cloisite®30B) was observed at ($2\theta = 5.08°$) with a corresponding interlayer spacing (d_{001}) of 1.73 nm. However, the diffraction peaks of the nanoclay in the PHBV/PBAT/silane-treated-RWF/nanoclay composites, shifted to lower angles in both solid ($2\theta = 2.38°$) and microcellular ($2\theta = 2.58°$) components with a corresponding interlayer spacing (d_{001}) of 3.53 and 3.27 nm for the solid and microcellular samples, respectively, indicating nanoclay intercalation occurred in the PHBV/PBAT composites [41]. Also. broad peaks at ($2\theta = 4.79°$) for solid components and at ($2\theta = 4.92°$) for microcellular components were observed in the XRD patterns, which originate from the appearance of a new basal reflection corresponding to a larger gallery height [42,43].

3.4. Mechanical properties

Fig. 6 and Table 5 show the results of the tensile tests (according to ASTM-D638) performed on the injection-molded solid and microcellular components of the PHBV/PBAT blend and its RWF and nanoclay filled composites. Properties such as specific modulus, energy-to-break (specific toughness), strain-at-break, and specific strength were measured. In the present study, the weight reductions of the microcellular components were 8.1%. 10.3%. 10.1%. and 9.6% for the PHBV/PBAT blend, PHBV/PBAT/untreated-RWF, PHBV/PBAT/silane-treated-RWF, PHBV/PBAT/silane-treated-RWF/nanoclay, respectively. Specific properties (i.e., specific strength, modulus, and toughness) were obtained by taking into account the density reduction

As shown in Fig. 6a, the addition of 10% untreated and silane-treated RWF increased the specific Young's modulus of both solid and microcellular samples significantly. The addition of untreated-RWF increased the Young's modulus by 85% and 28% for the solid and microcellular components, respectively. Silane-treatment did not cause any difference in the Young's modulus of the solid composites, but induced a slight increase in the microcellular composites. In addition, the addition of 2% nanoclay to the PHBV/PBAT/silane-treated-RWF composites did not affect the Young's modulus of either solid or microcellular components.

In general, the tensile strength of filled composites is found to decline when compared with their virgin polymer [44]. However, as shown in Table 5 and Fig. 6b, adding 10% RWF increased the specific tensile strength of both solid and microcellular components and a higher increase in the untreated-RWF composite was observed in the microcellular components compared with silane-treated-RWF composite. Similar to the Young's modulus, adding 2% nanoclay to

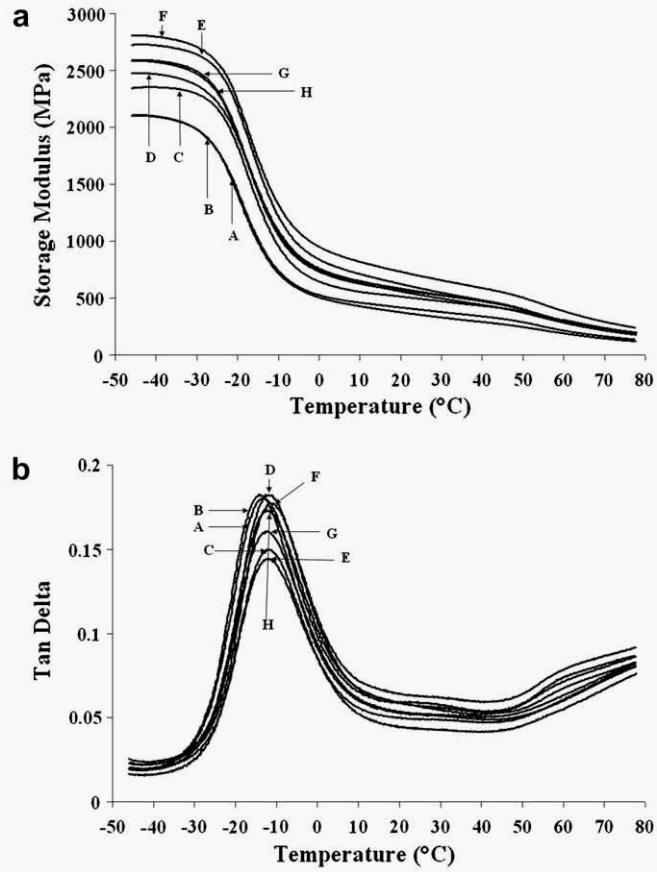

Fig. 7. Viscoelastic properties of the solid and microcellular PHBV/PBAT blend and PHBV/PBAT/RWF/nanoclay composites: (A) PHBV/PBAT blend (solid); (B) PHBV/PBAT blend (microcellular): (C) PHBV/PBAT/untreated-RWF composite (solid); (D) PHBV/PBAT/ PHBV/PBAT/untreated-RWF composite (microcellular); (E) PHBV/PBAT/silane-treated-RWF composite (solid): (F) PHBV/PBAT/silane-treated-RWF composite (microcellular): (G) PHBV/PBAT/silane-treated-RWF/nanoclay composite (solid): and (H) PHBV/PBAT/silane-treated-RWF/nanoclay composite (microcellular); (a) storage modulus as a function of temperature; (b) loss factor (Tan-δ) as a function of temperature.

Table 6
Numeric data of the area underneath the Tan-δ peak of the solid and microcellular PHBV/PBAT blend and its RWF/nanoclay composites.

Sampler		Area under the Tan-δ curve (°C)	T_g (°C)
PHBV/PBAT	Solid	5.3	−13.2
	Microcellular	5.3	−14.0
PHBV/PBAT + 10% untreated-RWF	Solid	4.2	−11.9
	Microcellular	5.3	−11.8
PHBV/PBAT+10%silane-treated-RWF	Solid	4.2	−12.0
	Microcellular	5.2	−12.1
PHBV/PBAT+10%silane-treated-RWF + 2% nanoclay	Solid	4.8	−11.2
	Microcellular	5.2	−11.9

the PHBV/PBAT/silane-treated-RWF composites did not induce a notable change in the strength of both solid and microcellular components either. Overall, the specific tensile strength of microcellular components was found to be less than that of their solid counterparts. This is because of certain large voids in the microcellular specimens that occurred due to the dynamic nature of the microcellular injection-molding process [45]. Such large voids act as stress concentrators, thereby decreasing mechanical properties.

As shown in Table 5 and Fig. 6c and d, the addition of 10% RWF resulted in a decrease in specific toughness and strain-at-break of the composites in both solid and microcellular components. This is due to the stiffening effect of the RWF. However, as shown in the Fig. 6, these composites still exhibit significant plastic deformation before fracture with a strain-at-break ranging between 12.8% and 30.7%. The specific toughness and strain-at-break of the untreated-RWF composite were higher than the silane-treated-RWF composite, particularly in the microcellular components. Similar to all other tensile properties, the addition of 2% nanoclay in the PHBV/PBAT/silane-treated-RWF composite did not induce notable changes in the specific toughness and strain-at-break for both solid and microcellular components. More significantly, while the specific toughness and strain-at-break of the microcellular PHBV/PBAT blend components were lower than their solid counterparts due to the presence of certain large voids in the microcellular components that act as regions of stress concentration, the specific toughness and strain-at-break of the microcellular RWF (both treated and untreated) composites were significantly higher than those of their solid counterparts, which may be attributed to the much smaller cell sizes and higher cell densities observed in these microcellular components due to RWF's microcell nucleating effects as discussed in the Morphology section of this paper [25]. Smaller cells hindered the formation of stress concentration regions and therefore an improvement in the specific toughness and strain-at-break were achieved [46].

3.5. Dynamic mechanical properties

DMA was used to study the viscoelastic properties of the solid and microcellular PHBV/PBAT blend and its RWF/nanoclay composites. The effect of temperature on the storage modulus of different samples is depicted in Fig. 7a. The storage modulus (E') of all the samples was observed to decline with increasing temperature. In the glassy region (−40 °C to −20 °C). a general trend of increased storage modulus with the addition of 10% untreated and silane-treated RWF to the PHBV/PBAT matrix was observed for both solid and microcellular components. The increase in storage modulus with the addition of RWF can be attributed to the restriction of polymer chains [41]. Moreover, the storage modulus of the PHBV/PBAT/silane-treated-RWF composite was apparently higher than that of the PHBV/PBAT/untreated-RWF composite for both solid and microcellular components. Finally, adding 2% nanoclay to the PHBV/PBAT/silane-treated-RWF composite led to a reduction in the storage moduli for both solid and microcellular components. For the same formulation, microcellular components had a slightly higher storage modulus compared with their solid counterparts [26].

Fig 7b and Table 6 show the Tan-δ curves and the numeric data of the area underneath the Tan-δ peak of all the samples. The area underneath Tan-δ peak represents the damping ability of the material; that is, the material's ability to absorb and dissipate energy [47]. As can be seen in Fig. 7b and Table 6, the area underneath the Tan-δ peak of the solid components decreased with the addition of untreated and silane-treated RWF compared with that of the pure PHBV/PBAT blend indicating that the filled composites have less energy absorbing ability than pure blends. This may be attributed to the fact that RWFs can act as stress concentrators thereby decreasing the damping ability. Moreover, the addition of 2% nanoclay in the PHBV/PBAT/silane-treated-RWF composite caused an increase in the area underneath the Tan-δ peak in the solid samples. On the other hand, the area underneath the Tan-δ peak of all three microcellular composites remained the same as that of the microcellular PHBV/PBAT blend indicating that all of the microcellular components possessed similar damping abilities.

Finally, it can be observed from Table 6 that with the addition of untreated and silane-treated RWF and nanoclay, the glass transition temperature (T_g) shifted to slightly higher temperatures which can be attributed to the limitation of chain mobility of the polymer matrix in the presence of fillers (RWF and nanoclay) [2].

4. Conclusion

Solid and microcellular components made of poly (3-hydroxybutyrate-*co*-3-hydroxyvalerate) (PHBV)/poly (butylene adipate-*co*-terephthalate) (PBAT) blend (weight ratio of PHBV: PBAT is 30:70) based on four different formulations were produced using both conventional and microcellular injection-molding processes: (a) PHBV/PBAT blend (b) PHBV/PBAT/untreated-RWF composite; (c) PHBV/PBAT/silane-treated-RWF composite; and (d) PHBV/PBAT/silane-treated-RWF/nanoclay composite. The addition of 10% RWF (untreated and silane-treated) decreased the cell size and increased the cell density in microcellular components compared to the neat PHBV/PBAT blend. The storage moduli increased in the PHBV/PBAT/RWF (untreated and silane-treated) composites compared with the neat PHBV/PBAT blend samples. Moreover, the silane-treated-RWF composite showed a higher storage modulus compared with untreated-RWF composite. Adding 10% untreated and silane-treated RWF generally increased the specific Young's modulus and tensile strength, but decreased the specific toughness and strain-at-break for both solid and microcellular samples. Unlike neat PHBV/PBAT blends, microcellular PHBV/PBAT/RWF (untreated and silane-treated) composites showed higher specific toughness and strain-at-break compared with their solid counterparts. It was found that the degree of PHBV crystallinity increased significantly with the addition of 10% untreated and silane-treated RWF compared to the PHBV/PBAT blend for both solid and microcellular components. Also it was observed that silane-treatment did not have any significant effect on the morphological, mechanical or thermal properties of the PHBV/PBAT/RWF composites. Additionally, the addition of 2% nanoclay. which exhibited an intercalated structure, in the PHBV/PBAT/silane-treated-RWF composite did not induce any significant changes in cell morphology (cell size and density) or mechanical properties, but did improve its thermal stability for both solid and microcellular components.

Acknowledgement

We gratefully acknowledge the financial support from the University of Wisconsin Solid Waste Research Program and the US Environmental Protection Agency.

References

[1] Mohanty AK, Misra M, Drzal LT. Sustainable bio-composites from renewable resources: opportunities and challenges in the green materials world. J Polym Environ 2002;10(1–2):19–26.
[2] Dufresne A, Dupeyre D, Paillet M. Lignocellulosic flour-reinforced poly(hydroxybutyrate-co-valerate) composites. J Appl Polym Sci 2003;87(8):1302–15.
[3] Chen GGQ. In: Smith R. editor. Biodegradable polymers for industrial applications. Cambridge (UK): Woodhead; 2005. p. 34.
[4] Yu L, Dean K, Lin L. Polymer blends and composites from renewable resources. Prog Polym Sci 2006;3(6):576–602.
[5] Gursel I, Balcik C, Arica Y, Akkus O, Akkas N, Hasirci V. Synthesis and mechanical properties of interpenetrating networks of polyhydroxybutyrate-co-hydroxyvalerate and polyhydroxyethyl methacrylate. Biomaterials 1998;19(13):1137–43.
[6] Avella M, Gaceva GB, Buzarovska A, Errico ME, Gentile G, Grozdanov A. Poly(3-hydroxybutyrate-co-3-hydroxyvalerate)-based biocomposites reinforced with kenaf fibers. J Appl Polym Sci 2007;104(5):3192–200.
[7] Lo WH, Yu J. Effects of the energy dissipation rate and surface erosion on the biodegradation of poly(hydroxybutyrate-co-hydroxyvalerate) and its blends with synthetic polymers in an aquatic medium. J Appl Polym Sci 2002;83(5):1036–45.
[8] Choi NS, Kim CH, Cho KY, Park JK. Morphology and hydrolysis of PCL/PLLA blends compatibilized with P(LLA-co-εCL) or P(LLA-b-εCL). J Appl Polym Sci 2002;86(8):1892–8.
[9] Kim CH, Cho KY, Choi EJ, Park JK. Effect of P(lLA-co-εCL) on the compatibility and crystallization behavior of PCL/PLLA blends. J Appl Polym Sci 2000;77(1):226–31.
[10] Chun YS, Kim WN. Thermal properties of blends of poly(hydroxybutyrate-co-hydroxyvalerate) and poly(styrene-co-acrylonitrile). J Appl Polym Sci 2000;77(3):673–9.
[11] Jenkins MJ, Cao Y, Howell L, Leeke GA. Miscibility in blends of poly(3-hydroxybutyrate-co-3-hydroxyvalerate) and poly(ε-caprolactone) induced by melt blending in the presence of supercritical CO_2.Polymer 2007; 48(21): 6304–10.
[12] Li J, Lai MF, Liu JJ. Control and development of crystallinity and morphology in poly(β-hydroxybutyrate-co-β-hydroxyvalerate)/poly(propylene carbonate) blends. J Appl Polym Sci 2005;98(3):1427–36.
[13] Kai W, He Y, Inoue Y. Fast crystallization of poly(3-hydroxybutyrate) and poly(3-hydroxybutyrate-co-3-hydroxyvalerate) with talc and boron nitride as nucleating agents. Polym Int 2005;54(5):780–9.
[14] Javadi A, Kramschuster AJ, Pilla S, lee J, Gong S, Turng LS. Processing and characterization of microcellular PHBV/PBAT blends. Polym Eng Sci 2010, in press, doi:10.1002/pen.21661.
[15] Ashori A. Wood–plastic composites as promising green-composites for automotive industries. Bioresour Technol 2008;99(11):4661–7.
[16] Rachtanapun P, Selke SEM, Matuana LM. Microcellular foam of polymer blends of HDPE/PP and their composites with wood fiber. J Appl Polym Sci 2003;88(12):2842–50.
[17] John MJ, Thomas S. Biofibres and biocomposites. Carbohydr Polym 2008;71(3):343–64.
[18] Samir MASA, Allioin F, Dufresne A. Review of recent research into cellulosic whiskers. Their Properties and Their Application in Nanocomposite Field Biomacromolecules 2005;6(2):612–26.
[19] Satyanarayana KG, Arizaga GGC, Wypych F. Biodegradable composites based on lignocellulosic fibers – an overview. Prog Polym Sci 2009;34(9):982–1021.
[20] Zhong Y, Poloso T, Hetzer M, Kee DD. Enhancement of wood/polyethylene composites via compatibilization and incorporation of organoclay particles. Polym Eng Sci 2007;47(6):797–803.
[21] Hristov VN, Vasileva ST. Deformation mechanisms and mechanical properties of modified polypropylene/wood fiber composites. Polym Compos 2004;25(5):521–6.
[22] Gong S, Yuan M, Chandra A, Winardi A, Osorio A, Turng LS. Microcellular injection molding. Int Polym Process 2005;2:202–14.
[23] Gong S, Turng LS, Park C, Liao L. Microcellular polymer nanocomposites for packaging and other applications. In: Mohanty A, Misra M, Nalwa HS. editor. Packaging nanotechnology. American Scientific Publishers; 2008. p.144 [chapter 6].
composites. J Appl Polym Sci 2009;111(1):37–47.
[25] Pilla S, Gong S, O'Neill E, Rowell RM, Krzysik AM. Polylactide-pine wood flour composites. Polym Eng Sci 2008;48(3):578–87.
[26] Pilla S, Kramschuster A, Gong S, Chandra A, Turng LS. Solid and microcellular polylactide-carbon nanotube nanocomposites. Int Polym Process 2007;5:418–28.
[27] Addonizio ML, Martuscelli E, Silvestre C. Study of the non-isothermal crystallization of poly(ethylene oxide)/poly(methyl methacrylate) blends. Polymer 1987;28(2):183–8.
[28] Nam PH, Maiti P, Okamoto M, Kotaka T, Nakayama T, Takada M, et al. Foam processing and cellular structure of polypropylene/clay nanocomposites. Polym Eng Sci 2002;42(9):1907–18.
[29] Naguib HE, Park CB, Reichelt N, Panzer U. Strategies for achieving ultra low-density polypropylene foams. Polym Eng Sci 2002;42(7):1481–92.
[30] Cui Y, Lee S, Noruziaan B, Cheung M, Tao J. Fabrication and interfacial modification of wood/recycled plastic composite materials. Composites: Part A 2008;39(4):655–61.
[31] McClurg RB. Design criteria for ideal foam nucleating agents. Chem Eng Sci 2004;59(24):5779–86.
[32] Matuana LM, Park CB, Balatinecz JJ. Cell morphology and property relationships of microcellular foamed pvc/wood-fiber composites. Polym Eng Sci 1998;38(11):1862–72.
[33] Masirek R, Kulinski Z, Chionna D, Piorkowska E, Pracella MJ. Composites of poly(ι-lactide) with hemp fibers: morphology and thermal and mechanical properties. J Appl Polym Sci 2007;105(1):255–68.
[34] Bruzaud S, Bourmaud A. Thermal degradation and (nano) mechanical behavior of layered silicate reinforced poly(3-hydroxybutyrate-co-3-hydroxyvalerate) nanocomposites. Polym Test 2007;26(5):652–9.
[35] Mohanty S, Nayak SK. Aromatic-aliphatic poly(butylene adipate-co-terephthalate) bionanocomposite: Influence of organic modification on structure and properties. Polym Compos 2009; Early View (Articles online in advance of print) Published Online: 17 Aug 2009.
[36] Wang S, Song C, Chen G, Guo T, Liu J, Zhang B, et al. Characteristics and biodegradation properties of poly(3-hydroxybutyrate-co-3-hydroxyvalerate)/organophilic montmorillonite (PHBV/OMMT) nanocomposite. Polym Degrad Stab 2005; 87(1): 69–76.
[37] Nishioka N, Hamabe S, Murakami T, Kitagawa T. Thermal decomposition behavior of miscible cellulose/synthetic polymer blends. J Appl Polym Sci 1998;69(11):2133–7.
[38] Suprakas S, Kazunobu Y, Masami O, Kazue U. Polylactide-layered silicate nanocomposite: a novel biodegradable material. Nano Lett 2002;2(10):1093–6.
[39] Bordes P, Pollet E, Avêrous L. Nano-biocomposites: biodegradable polyester/nanoclay systems. Prog Polym Sci 2009;34(2):125–55.
[40] Lim ST, Hyun YH, Lee CH, Choi HJ. Preparation and characterization of microbial biodegradable poly(3-hydroxybutyrate)/organoclay nanocomposite. J Mater Sci Lett 2003;22(4):299–302.
[41] Li T, Turng LS, Gong S, Erlacher K. Polylactide, nanoclay, and core-shell rubber composites. Polym Eng Sci 2006;46(10):1419–27.
[42] Li X, Park HM, Lee JO, Ha CS. Effect of blending sequence on the microstructure and properties of PBT/EVA-g-MAH/organoclay ternary nanocomposites. Polym Eng Sci 2002;42(11):2156–64.
[43] Miao L, Qiu Z, Yang W, Ikehara T. Fully biodegradable poly(3-hydroxybutyrate-co-hydroxyvalerate)/poly(ethylene succinate) blends: Phase behavior, crystallization and mechanical properties. React Funct Polym 2008;68(2):446–57.
[44] Zuiderduin WCJ, Westzaan C, Huetink J, Gaymans RJ. Toughening of polypropylene with calcium carbonate particles. Polymer 2003;44(1):261–75.
[45] Kramschuster A, Gong S, Turng LS, Li T, Li T. Injection-molded solid and microcellular polylactide and polylactide nanocomposites. J Biobased Mater Bioenergy 2007;1(1):37–45.
[46] Collias DI, Baird DG. Tesile toughness of microcellular foams of polystyrene, styrene-acrylonitrile copolymer, and polycarbonate, and the effect of dissolved gas on the tensile toughness of the same polymer matrices and microcellular foams. Polym Eng Sci 1995;35(14):1167–77.
[47] Pothan LA, Oommen Z, Thomas S. Dynamic mechanical analysis of banana fiber reinforced polyester composites. Compos Sci Technol 2003;63(2):283–93.